

# A New Physically-Based Fully-Realizable Nonequilibrium Reynolds Stress Closure for Turbulent Flow RANS Modeling.

Peter E. Hamlington and Werner J.A. Dahm

*Laboratory for Turbulence and Combustion (LTC)*

*Department of Aerospace Engineering, The University of Michigan*

*Ann Arbor, MI, 48109-2140, USA*

Based on the physics underlying turbulence anisotropy in the equilibrium and nonequilibrium limits, a new physically-based, fully-realizable, nonequilibrium  $k - \epsilon$  RANS model has been developed. The model is based on an effective strain rate tensor that accounts for the strain history to which the turbulence has been subjected. This new model is applied to four distinctly different test cases for which the nonequilibrium history integral can be evaluated analytically. Results obtained from this new closure model show dramatically improved agreement with experimental and computational data when compared with the standard  $k - \epsilon$  (SKE) model, without the need to vary any model parameters. The introduction of a nonequilibrium effective strain rate allows this new model to be applied within a similar framework as currently used for two-equation eddy viscosity models, thereby permitting relatively simple implementation in existing CFD codes.

## Nomenclature

$k$	Turbulent kinetic energy	$b_{ij}$	Reynolds stress anisotropy tensor
$\epsilon$	Turbulent dissipation rate	$\tau_T$	Turbulence time scale
$S_{ij}$	Mean strain rate tensor	$\tau_S$	Mean strain time scale
$\overline{u'_i u'_j}$	Reynolds stress tensor	$\Lambda_m$	Memory time scale
$\nu_T$	Turbulent eddy viscosity	$\tilde{S}_{ij}$	Effective mean strain rate tensor
$P_k$	Turbulence kinetic energy production	$\Omega_{ij}$	Mean rotation rate tensor

## I. Introduction

Due to the overwhelming computational resources currently required for large eddy simulation, the vast majority of engineering simulations of turbulent flows will continue to be done in the foreseeable future with Reynolds-averaged Navier Stokes (RANS) codes. In the RANS approach, the single-point second-order velocity fluctuation correlations (i.e., the Reynolds stresses) prevent closure of the governing equations without the addition of one or more additional equations that ultimately relate the Reynolds stress tensor to the mean flow pressure and velocity components. Finding accurate yet computationally feasible forms of such closure approximations is the primary challenge in turbulence modeling.

The most accurate RANS closures today are “Reynolds stress transport” (RST) models, wherein a system of coupled partial differential equations is solved for the six independent components of the Reynolds stress tensor. While in principle the RST equations contain all of the relevant turbulence physics that affect the evolution of the Reynolds stresses, these equations introduce yet higher-order correlations that ultimately must somehow be modeled. Moreover, numerical integration of the six coupled partial differential equations introduces an additional computational load that, while reasonably manageable with today’s computers, originally hindered adoption of the RST approach in the most widely used CFD codes. For these reasons, it has become standard practice to use simple algebraic “linear eddy viscosity models” (LEVMs) to close the RANS equations.

In LEVMs, the Reynolds stresses are modeled via the Boussinesq “gradient transport” hypothesis, wherein a scalar eddy viscosity is used to linearly relate the stresses with the mean strain rate tensor. In two-equation LEVMs, the eddy viscosity is calculated using two differential transport equations, and in the most widely used two-equation model – namely the standard  $k - \epsilon$  (SKE) model – transport equations are solved for the turbulence kinetic energy  $k$  and its dissipation rate  $\epsilon$ .<sup>1</sup> However, these two equations also introduce fluctuation correlations that must somehow be modeled. Despite a strong reliance on unphysical *ad hoc* modeling in the transport equations for  $k$  and  $\epsilon$ , the SKE model remains the most popular closure method due to its computational simplicity and its modest success in simulating a surprisingly wide range of flows. Numerous variations on the SKE model have been proposed, typically by recasting the eddy viscosity in variables other than  $k$  and  $\epsilon$ , but all such two-equation LEVMs show roughly similar levels of inaccuracy over a broad spectrum of turbulent flows.

The errors inherent in two-equation LEVMs come from two sources. The first are the higher-order correlations that appear in the additional transport equations for the two variables in which the eddy viscosity is cast, which must typically be modeled by various *ad hoc* assumptions. The second and even more fundamental source is the linear gradient transport hypothesis itself. The assumption of a *scalar* eddy viscosity, and the further assumption that the Reynolds stresses depend on only the *instantaneous* mean strain rate tensor, are known to be important shortcomings of LEVMs.<sup>2–4</sup> In particular, modeling the stresses in terms of the instantaneous mean strain rate tensor renders LEVMs inaccurate in nonequilibrium flows, where the turbulence undergoes rapid time-dependent straining. Simple examples of such flows include suddenly-sheared homogeneous turbulence, periodically-sheared turbulence, and turbulence that is rapidly strained and destrained. To fully account for nonequilibrium effects, the model for the Reynolds stresses must in principle account for the entire strain history, and cannot be based simply on the current strain state.

Given the deficiencies of the linear gradient transport hypothesis, various *nonlinear* eddy viscosity models (NLEVMs) have been developed to address some of the shortcomings of LEVMs. In NLEVMs, it is assumed that the Reynolds stresses depend on all possible tensorial combinations of the mean strain and rotation rate tensors, resulting in a stress-strain constitutive equation similar to those found in continuum mechanics for viscoelastic materials.<sup>5–7</sup> Closure of the RANS equations with such models thus reduces to determining the coefficients in the tensorial expansion. Many researchers have used physical considerations such as rapid distortion theory, material frame indifference, and full realizability to determine the coefficients (*e.g.*, Shih *et al.*<sup>8</sup>), although in recent years it has become popular to connect the constitutive equation and its coefficients to the Reynolds stress transport equation itself.<sup>9,10</sup>

By including the mean rotation rate terms in the Reynolds stress closure, and due to the anisotropic eddy viscosity that results from the nonlinear higher-order tensorial combinations of the stress and rotation rate tensors, NLEVMs succeed in many of the flows where models based on the linear gradient transport hypothesis fail. However, nonlinear models of the same order derived by different methods often have inconsistent expansion coefficients, depending on the physical considerations used to achieve the closure.<sup>11</sup> Moreover, most NLEVMs only relate the Reynolds stresses to the *instantaneous* mean strain and rotation rate tensors, rendering these models as insensitive to nonequilibrium effects as classical LEVMs. Speziale,<sup>12</sup> Yakhot *et al.*,<sup>13</sup> Yoshizawa and Nisizima,<sup>14</sup> and Huang and Rajagopal<sup>15</sup> have attempted to include nonequilibrium effects with some success, but because the resulting models cannot be readily substituted for the LEVMs found in the most widely used CFD codes, these approaches have not found widespread applicability or popularity. To date, despite their shortcomings, the SKE model and its variants remain the most popular closure methods for simulating turbulent flows of engineering interest.

Here we use fundamental turbulence physics to develop a new NLEVM that correctly captures nonequilibrium effects due to the strain rate history to which the turbulence has been subjected, but the resulting model is in a form that can be readily substituted in CFD codes for standard models such as SKE and its variants. In contrast to many previous NLEVMs, the present model does not assume an *a priori* form of the turbulence constitutive equation, and instead acquires its nonlinearity through consideration of the physics underlying turbulence anisotropy in the nonequilibrium limit. By accounting for nonequilibrium effects, substantial improvements are achieved over the SKE model in a wide range of test cases. At the same time, the new model retains much of the SKE framework, in particular the  $k$  and  $\epsilon$  transport equations, and thus provides an improved algebraic Reynolds stress closure that is relatively simple to incorporate in existing CFD codes.

The paper is organized as follows. Section II first presents a description of turbulence anisotropy in the

equilibrium limit of the standard  $k - \epsilon$  model. Section III then describes the relation between nonequilibrium effects and the turbulence anisotropy, and uses this to formulate a nonequilibrium  $k - \epsilon$  (NKE) model in terms of an effective strain tensor that accounts for the past strain history to which the turbulence has been subjected. In Section IV, the resulting NKE model is applied to a variety of nonequilibrium turbulent flows, including (i) impulsively-sheared homogeneous turbulence, (ii) periodically-sheared turbulence, (iii) turbulence that is rapidly strained and then destrained, and (iv) the shock-turbulence interaction. For all these cases, the effective strain tensor in the NKE model can be evaluated analytically, and either DNS data or experimental data are available for model validation. Results obtained for the turbulence anisotropy from the NKE model are seen to be in good agreement with the validation data. Section V shows that full realizability constraints can be imposed on the NKE model, which allows the model to be applied at very large shear values such as in near-wall turbulence. Section VI then discusses a number of additional considerations, including the evaluation of the history integral in a CFD code, and the relation between the present NKE model and various prior NLEVMs.

## II. Equilibrium Turbulence Anisotropy

Averaging of the incompressible continuity and Navier-Stokes equations leads to the single-point RANS system of equations commonly used in turbulence modeling

$$\frac{\partial \bar{u}_i}{\partial x_i} = 0 \quad \text{and} \quad \frac{\partial \bar{u}_i}{\partial t} + \bar{u}_j \frac{\partial \bar{u}_i}{\partial x_j} = \frac{D\bar{u}_i}{Dt} = -\frac{\partial \bar{p}}{\partial x_i} + \frac{\partial}{\partial x_j} \left[ 2\nu S_{ij} - \overline{u'_i u'_j} \right], \quad (1)$$

where  $D/Dt$  denotes the mean flow material derivative,  $\bar{u}_i$  is the mean velocity field,  $u'_i$  the fluctuation velocity field,  $\bar{p}$  the mean pressure,  $\nu$  the molecular viscosity, and  $S_{ij}$  is the symmetric mean strain rate tensor, given by

$$S_{ij} = \frac{1}{2} \left( \frac{\partial \bar{u}_i}{\partial x_j} + \frac{\partial \bar{u}_j}{\partial x_i} \right). \quad (2)$$

The Reynolds stresses  $\overline{u'_i u'_j}$  appearing in (1) prevent closure of the governing equations and are commonly modeled as the sum of isotropic and anisotropic parts as

$$\overline{u'_i u'_j} = \frac{2}{3} k \delta_{ij} - (\overline{u'_i u'_j})_{dev}, \quad (3)$$

where  $k = \frac{1}{2} \overline{u'_i u'_i}$  is the turbulence kinetic energy, and  $(\overline{u'_i u'_j})_{dev}$  is the anisotropic contribution to the stresses. In isotropic turbulence the deviatoric stresses are zero and the full Reynolds stress tensor is

$$\overline{u'_i u'_j} = \frac{2}{3} k \delta_{ij}, \quad (4)$$

where only the on-diagonal Reynolds stresses are non-zero. Since the trace of the Reynolds stress tensor must equal  $2k$ , the trace of the anisotropic stresses vanishes so that

$$(\overline{u'_i u'_i})_{dev} = 0, \quad (5)$$

whether or not the turbulence is isotropic.

Since the isotropic contribution to the Reynolds stresses in (3) is known, only the anisotropic stresses must be modeled in order to close the RANS equations. In LEVMs the anisotropic stresses are commonly expressed using the gradient transport hypothesis

$$(\overline{u'_i u'_j})_{dev} = \nu_T \left( \frac{\partial \bar{u}_i}{\partial x_j} + \frac{\partial \bar{u}_j}{\partial x_i} \right) = 2\nu_T S_{ij}, \quad (6)$$

where  $\nu_T$  is the eddy viscosity. Typically  $\nu_T$  is modeled as the product of length and velocity scales characteristic of the turbulent flow, and in the SKE model is given by

$$\nu_T = C_\mu \frac{k^2}{\epsilon}, \quad (7)$$

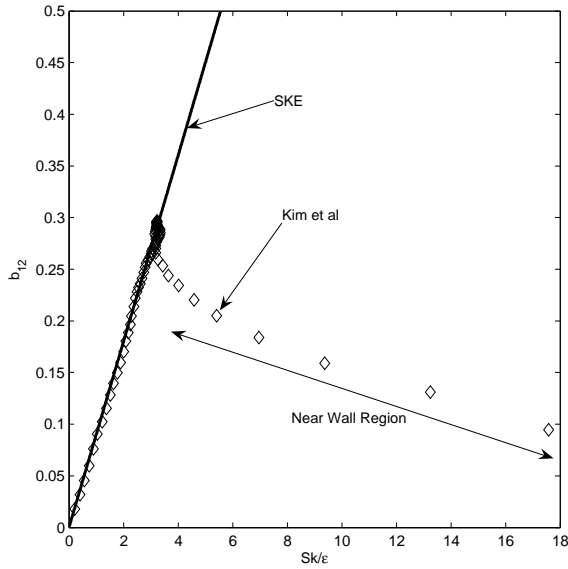


Figure 1. Anisotropy in a turbulent channel flow. The SKE closure agrees with the computational data of Kim *et al.*<sup>16</sup> for small values of  $Sk/\epsilon$  outside the near-wall region.

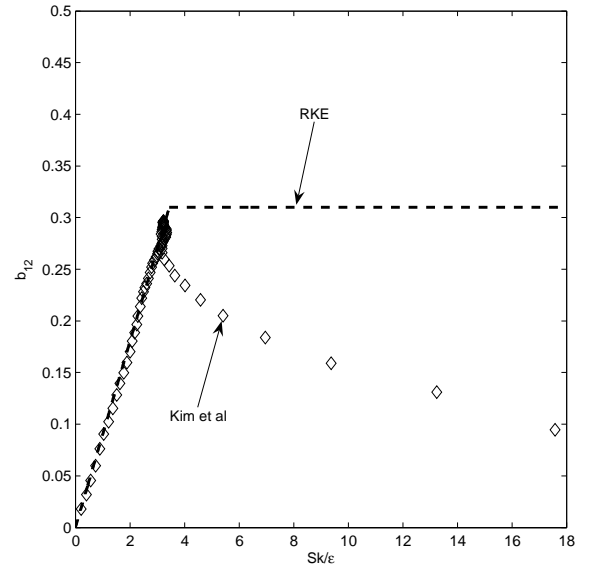


Figure 2. Channel flow anisotropy predicted by the RKE closure, where the anisotropy is limited for the large values of  $Sk/\epsilon$  present in the near wall region.

where  $C_\mu$  is a constant and  $\epsilon$  is the turbulence kinetic energy dissipation rate. Closure is achieved through the addition of the two modeled transport equations

$$\frac{Dk}{Dt} = P_k - \epsilon + \frac{\partial}{\partial x_j} \left[ \left( \nu + \frac{\nu_T}{\sigma_k} \right) \frac{\partial k}{\partial x_j} \right], \quad (8)$$

$$\frac{D\epsilon}{Dt} = C_{\epsilon 1} P_k \frac{\epsilon}{k} - C_{\epsilon 2} \frac{\epsilon^2}{k} + \frac{\partial}{\partial x_j} \left[ \left( \nu + \frac{\nu_T}{\sigma_\epsilon} \right) \frac{\partial \epsilon}{\partial x_j} \right], \quad (9)$$

where  $P_k$  is the kinetic energy production rate defined as

$$P_k = -\overline{u'_i u'_j} S_{ij}. \quad (10)$$

Standard values for the SKE model constants are<sup>1</sup>

$$C_\mu = 0.09, \quad C_{\epsilon 1} = 1.44, \quad C_{\epsilon 2} = 1.92, \quad \sigma_k = 1, \quad \text{and} \quad \sigma_\epsilon = 1.3. \quad (11)$$

The resulting expression for the anisotropic stresses in the SKE model is then

$$\overline{(u'_i u'_j)}_{dev} = 2C_\mu \frac{k^2}{\epsilon} S_{ij} = 2kC_\mu \frac{Sk}{\epsilon} \frac{S_{ij}}{S}, \quad (12)$$

where  $S = (S_{ij} S_{ij})^{1/2}$  is the second invariant of the mean strain rate tensor. The SKE Reynolds stress closure is not typically written in a manner that explicitly shows the linear dependence on  $Sk/\epsilon$ , but as will be seen in the next section, the parameter  $Sk/\epsilon$  is physically related to the magnitude of the turbulence anisotropy, and the formulation above is therefore informative.

The closure in (12) is relatively successful in equilibrium turbulent flows such as channel or other thin shear flows where material derivatives of flow properties like  $k$  and  $\epsilon$  are small. Figure 1 shows the agreement between the anisotropy predicted by (12) and the DNS channel flow data of Kim *et al.*,<sup>16</sup> where the anisotropy tensor is defined as

$$b_{ij} = -\frac{\overline{(u'_i u'_j)}_{dev}}{2k}. \quad (13)$$

From Figure 1 it is clear that the SKE model and the data agree well for small values of  $Sk/\epsilon$ , but the model departs significantly from the data for large values of  $Sk/\epsilon$  occurring in the near wall region. This issue is

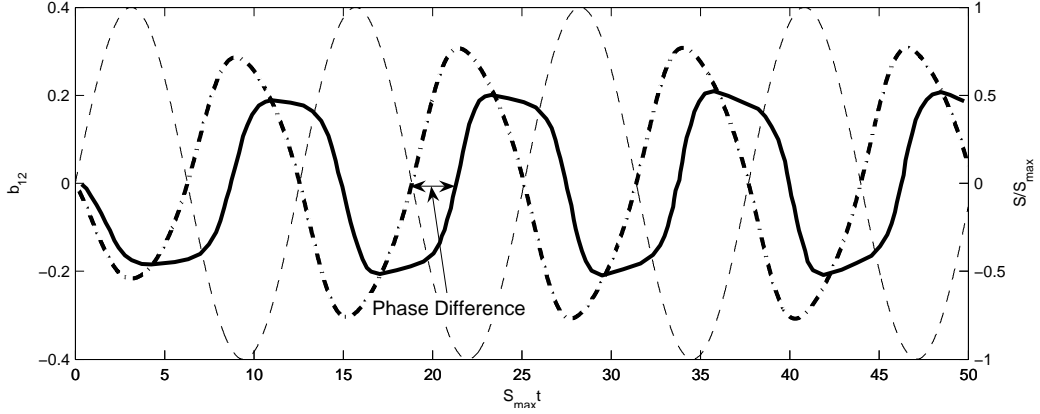


**Figure 3.** Plot of  $b_{12}$  for periodically sheared turbulence with  $\omega/S_{max} = 0.5$  and  $S_{max}k_0/\epsilon_0 = 3.3$ . The SKE closure (dash-dot line) does not agree with either the amplitude or phase of the computational results from Yu and Girimaji<sup>17</sup> (solid line). The applied shear is represented by the thin dashed line.

partly addressed by the realizable  $k - \epsilon$  (RKE) model, where the constant  $C_\mu$  appearing in (12) is limited in the high  $Sk/\epsilon$  limit as

$$C_\mu = \begin{cases} 0.09 & \text{for } 0 \leq \frac{Sk}{\epsilon} \leq 3.4 \\ 0.31 \left(\frac{Sk}{\epsilon}\right)^{-1} & \text{for } 3.4 < \frac{Sk}{\epsilon} < \infty \end{cases}. \quad (14)$$

This limits the unbounded increase in the anisotropy predicted by the SKE model, but still does not follow the computational data of Kim *et al.* in the near wall region where  $Sk/\epsilon$  is large, as shown in Figure 2. Wall functions are typically used to force better agreement in the near wall region.

### III. The Nonequilibrium $k - \epsilon$ (NKE) Model

Neglecting the near wall region in Figure 1, the general success of the SKE model in equilibrium flows motivates the use of (12) as the foundation on which further model improvements can be based. In general, the SKE closure in (12) performs well in equilibrium flows, but does significantly less well in nonequilibrium flows where Lagrangian flow properties change rapidly. An example of this is seen in periodically-sheared homogeneous turbulence, for which Yu and Girimaji<sup>17</sup> have recently obtained DNS data. In this case, the velocity gradient and strain rate tensors are

$$\frac{\partial \bar{u}_i}{\partial x_j}(t) = S_{max} \sin(\omega t) \delta_{i1} \delta_{j2} \quad \Rightarrow \quad S_{ij}(t) = \frac{S_{max}}{2} \sin(\omega t) [\delta_{i1} \delta_{j2} + \delta_{i2} \delta_{j1}], \quad (15)$$

where  $\omega$  is the applied shearing frequency. Applying the conventional SKE closure to this flow, the only nonzero components of the anisotropy tensor are

$$b_{12}(t) = b_{21}(t) = -C_\mu \frac{k}{\epsilon} S_{12}(t) \quad (16)$$

and the homogeneous  $k$  and  $\epsilon$  transport equations become

$$\frac{\partial k}{\partial t} = -4kb_{12}S_{12} - \epsilon \quad \text{and} \quad \frac{\partial \epsilon}{\partial t} = -4C_{\epsilon 1}\epsilon b_{12}S_{12} - C_{\epsilon 2}\frac{\epsilon^2}{k}, \quad (17)$$

where the turbulent kinetic energy production appearing in Eqs. (8) and (9) has been written in terms of the anisotropy tensor as

$$P_k = -\overline{u'_i u'_j} S_{ij} = -2kb_{ij}S_{ij}. \quad (18)$$

This system of coupled ordinary differential equations can be integrated numerically for the three unknowns  $k$ ,  $\epsilon$ , and  $b_{12}$ , yielding the anisotropy evolution in Figure 3 for a shearing frequency of  $\omega/S_{max} = 0.5$  with  $S_{max}k_0/\epsilon_0 = 3.3$ . When compared with the results of Yu and Girimaji, Figure 3 shows that the SKE model does not agree with either the amplitude or phase of the computationally obtained anisotropy (for larger

values of  $\omega/S_{max}$  there is even an offset in the computational results which the SKE model also does not capture).

The poor phase agreement in Figure 3 results from the fact that the anisotropy in the SKE model is assumed to depend on the *instantaneous* strain tensor, so that when  $S/S_{max}$  is zero the anisotropy is also zero. The phase difference, or lag, between the applied strain and turbulence response is seen in many other flows as well, such as homogeneous sheared turbulence, turbulence that is successively strained and destrained, and even the decay of turbulence behind a grid, where a nonzero anisotropy persists after the grid straining ends. Nonequilibrium effects must be included in the closure model to correctly account for the lag between the applied strain and anisotropy.

### III.A. Physics of Turbulence Anisotropy

Both equilibrium and nonequilibrium turbulence anisotropy can be understood from a quasi-Lagrangian standpoint, where the turbulence is viewed as being composed of numerous material elements convecting with the mean flow at velocity  $\bar{u}_i$ . Each element contains vortical structures that produce a combined fluctuation velocity field  $u'_i(\mathbf{x})$ , from which a single Reynolds stress tensor  $\overline{u'_i u'_j}$  associated with the element as a whole is obtained.

In this quasi-Lagrangian picture, the anisotropy is determined by the alignment of the vortical structures in the fluid element relative to the eigenvectors of the strain rate tensor that acts on the element. Maximum anisotropy is obtained when the vortical structures are fully aligned, while isotropy results when the structures are randomly aligned. Thus in the quasi-Lagrangian picture, an understanding of the alignment dynamics leads to an understanding of the turbulence anisotropy.

Fundamentally, the relative alignment of the vortical structures is determined by the competing effects of alignment by the externally imposed mean strain rate tensor and misalignment by the local strain induced by vortical structures within the element. Specifically, the mean strain tends to align the vortical structures with the direction of the most extensional eigenvector of the mean strain rate tensor, while the local and self-induced strain tends to ruin the alignment with this eigenvector.

The degree of vortical structure alignment can be quantified by considering the ratio of the misalignment (or turbulence) time scale  $\tau_T = k/\epsilon$  to the mean strain time scale  $\tau_S = 1/S$ , such that the anisotropy magnitude is characterized by the parameter

$$\frac{\tau_T}{\tau_S} = \frac{Sk}{\epsilon}. \quad (19)$$

If the turbulence time scale is small compared to the mean flow time scale ( $Sk/\epsilon$  is small), then the vortical structures are misaligned more rapidly than they are aligned, resulting in isotropic turbulence. On the other hand, if the mean flow time scale is small compared to the turbulence time scale ( $Sk/\epsilon$  is large), then the vortical structures are aligned more rapidly than they are misaligned and maximum anisotropy results. Thus the mean strain rate tensor determines the direction and degree of turbulence anisotropy.

In equilibrium turbulence, the mean strain rate imposed on each fluid element changes very slowly as the elements move with the mean flow, and the vortical structure alignment depends completely on the instantaneous value of  $S_{ij}$  experienced by the element. The formulation of the equilibrium SKE closure in (12) is therefore justified by the quasi-lagrangian picture of turbulence, where the anisotropy magnitude is explicitly determined by the instantaneous value of  $Sk/\epsilon$ , and the elements of the Reynolds stress tensor are proportional to the elements of the instantaneous mean strain tensor  $S_{ij}$ . Moreover, the linear dependence of the anisotropy magnitude on  $Sk/\epsilon$  in the SKE model is qualitatively consistent with the relationship between the anisotropy and  $Sk/\epsilon$  developed in the quasi-lagrangian picture of turbulence (that is, for example, as  $Sk/\epsilon$  increases the anisotropy magnitude also increases).

In nonequilibrium turbulence, however, it is no longer appropriate to let the anisotropy depend on the instantaneous values of  $S_{ij}$  and  $Sk/\epsilon$ . For example, consider isotropic turbulence that is suddenly subjected to the shear  $S_{12} = S_{21} = S/2$  at time  $t = 0$ . Since the applied shear is known, the  $k$  and  $\epsilon$  transport equations can be integrated numerically using the SKE model, and Figure 4 shows the resulting turbulence kinetic energy evolution compared with the LES data of Bardina *et al.*<sup>18</sup> It is clear that the modeled kinetic energy is over-predicted due to excessive initial kinetic energy production, which is in turn caused by initially over-predicted turbulence anisotropy.

The over-predicted anisotropy arises because the applied shear does not instantly align all of the initially isotropic vortical structures with the most extensional eigenvector of the mean strain rate tensor. This much

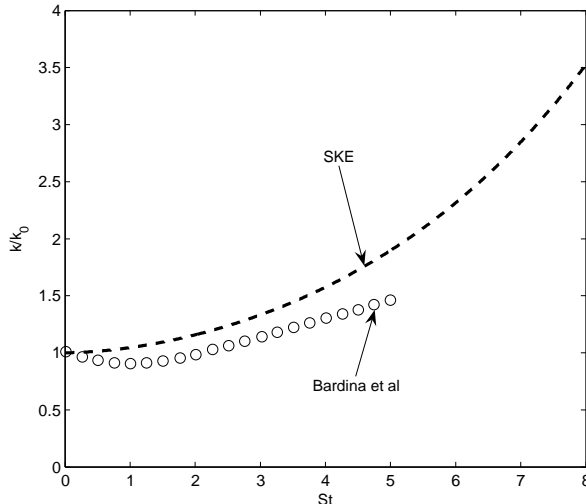


**Figure 4.** Evolution of the turbulent kinetic energy  $k/k_0$  for initially isotropic turbulence that is homogeneously sheared, where  $\epsilon_0/Sk_0 = 0.296$ . Compared to the LES data of Bardina *et al.*,<sup>18</sup> the SKE model over-predicts the kinetic energy for all times.

is apparent from the inviscid vorticity transport equation

$$\frac{D\omega_i}{Dt} = S_{ij}\omega_j, \quad (20)$$

where alignment with the most extensional eigenvector proceeds on a time scale  $\tau_S = 1/S$ . The random self-induced straining, which proceeds on the turbulence time scale  $\tau_T = k/\epsilon$ , tends to further slow the alignment process. Moreover, once the shear is applied the vortical structures do not immediately reach a degree of relative alignment that can be fully characterized by the instantaneous value of  $Sk/\epsilon$  (as in the equilibrium SKE closure). Rather, they retain some memory of their initially isotropic state, and the anisotropy magnitude relaxes to its final value in some finite, non-zero, time. For suddenly sheared homogeneous isotropic turbulence, the anisotropy at initial times is therefore not as large as the SKE closure predicts, and the real kinetic energy production is lower. Thus the quasi-Lagrangian picture validates the SKE closure as a reasonable model for anisotropy near the equilibrium limit, and motivates a physically-valid description of the relaxation process by which vortical structures approach their equilibrium anisotropy state.

### III.B. The Effective Strain Rate

The anisotropy relaxation process can be understood by dividing the vortical structures in each fluid element into separate ensembles characterized by different mean strain rates. For example, immediately after the straining is applied in homogeneous shear turbulence, only a fraction of the vortical structures have reached an anisotropy state determined by the instantaneous value of  $S_{ij}$ , while the rest of the vortical structures are still in an anisotropy state determined by the previous value of the mean strain tensor (which is, incidentally,  $S_{ij} = 0$ ). Thus, the vortical structures can be divided into one ensemble with anisotropy determined by  $S_{ij}(t)$  and another ensemble with anisotropy determined by  $S_{ij}(t - \Delta t)$ , where in both cases an equilibrium expression (such as the SKE closure) is used for the ensemble anisotropy. Over time, the fraction of vortical structures that have reached the new anisotropy state increases, until all of the structures have effectively reached the new state when  $t \gg \Lambda_m$ , where  $\Lambda_m$  is a memory time scale that characterizes how quickly the vortical structures ‘forget’ about their past. At any time, the total anisotropy in the fluid element is equal to the weighted average of the anisotropy associated with all ensembles, where the weighting is determined by the size of each ensemble.

The physics of the anisotropy ensembles can be incorporated within the framework of the SKE closure in (12) by defining an effective strain rate  $\tilde{S}_{ij}$ , so that

$$b_{ij} = -C_\mu \frac{k}{\epsilon} \tilde{S}_{ij} = -C_\mu \frac{\tilde{S}k}{\epsilon} \frac{\tilde{S}_{ij}}{\tilde{S}}, \quad (21)$$

where  $\tilde{S}$  is the second invariant of the effective strain tensor. Due to the linear relationship between the anisotropy and the mean strain rate in the SKE closure, a weighted average of the ensemble anisotropies is equivalent to a weighted average of the strain rates that characterize the anisotropy in each ensemble. The effective strain rate is thus defined as the normalized weighted average over the past straining history, so that

$$\tilde{S}_{ij}(t) = g_0 S_{ij}(t) + g_1 S_{ij}(t - \Delta t) + \dots = \sum_{i=0}^{\infty} g_i S_{ij}(t - i\Delta t), \quad (22)$$

where the  $g_i$  are non-dimensional history weighting coefficients, with

$$\sum_{i=0}^{\infty} g_i = 1. \quad (23)$$

This is written in equivalent continuous form via the convolution integral

$$\tilde{S}_{ij}(t) = \int_{-\infty}^t h(t - \tau) S_{ij}(\tau) D\tau, \quad (24)$$

where now  $h(\tau)$  is a history function with units of  $t^{-1}$  normalized so that

$$\int_0^{\infty} h(\tau) d\tau = 1. \quad (25)$$

By definition  $h(\tau)$  is a maximum at  $\tau = 0$  and  $h(\tau) \rightarrow 0$  as  $\tau \rightarrow \infty$ . With  $h(\tau)$  of this form the effective strain rate is most affected by strain rates near time  $t$ , while all past strain rates have a lesser impact. Note that the integral in (24) is with respect to the material differential  $D\tau$  because the strain rate experienced by a fluid element varies due to both temporal unsteadiness and convection by the mean flow.<sup>5</sup> Thus, by ‘straining history’ we specifically mean the history of the strain rates experienced by a quasi-Lagrangian fluid element.

The history function is loosely connected to the temporal autocorrelation of the turbulence, and this motivates an exponential form as

$$h(\tau) = \frac{1}{\Lambda_m} e^{-\tau/\Lambda_m}, \quad (26)$$

where  $\Lambda_m$  is the memory time scale. The effective strain rate is thus written in full form as

$$\tilde{S}_{ij}(t) = \int_{-\infty}^t \frac{e^{-(t-\tau)/\Lambda_m}}{\Lambda_m} S_{ij}(\tau) D\tau. \quad (27)$$

A natural time scale for  $\Lambda_m$  is the turbulence time scale  $\tau_T = k/\epsilon$ , where the randomizing effect of the turbulence is taken as the source of the vortical structure memory loss. While it is possible that the magnitude of the mean strain tensor, and in particular the parameter  $Sk/\epsilon$ , could play a role in setting  $\Lambda_m$  for flows where  $Sk/\epsilon$  is large, it is sufficient here to define

$$\Lambda_m = C_\Lambda \frac{k}{\epsilon}. \quad (28)$$

It will be seen herein that a universal value of  $C_\Lambda = 0.26$  gives good agreement with widely differing nonequilibrium test cases.

### III.C. The NKE Model

The nonequilibrium model developed in the preceding sections can be summarized by the system of equations

$$\overline{u'_i u'_j} = \frac{2}{3} k \delta_{ij} - C_\mu \frac{\tilde{S} k}{\epsilon} \frac{\tilde{S}_{ij}}{\tilde{S}}, \quad (29)$$

where the effective strain rate is

$$\tilde{S}_{ij}(t) = \int_{-\infty}^t \frac{e^{-(t-\tau)/\Lambda_m}}{\Lambda_m} S_{ij}(\tau) D\tau \quad (30)$$

and the memory time scale is

$$\Lambda_m = C_\Lambda \frac{k}{\epsilon}; \quad C_\Lambda = 0.26. \quad (31)$$

Consistent with the general framework of the SKE model, the system of equations is closed using the  $k$  and  $\epsilon$  transport equations in (8) and (9), where the constants appearing in the equations are defined in (11). The model represented by Eqs. (29) - (31) will be referred to as the nonequilibrium  $k-\epsilon$  (NKE) model. In Section IV, this model is applied to predict the turbulence response in four distinctly different nonequilibrium test cases for which the effective strain rate in (30) can be determined analytically. Section VI describes how this history integral can be evaluated for implementation in standard RANS modeling codes.

Before continuing, a few general comments on the NKE model should be mentioned. First, as noted in Eq. (5), the trace of the anisotropic stresses in any valid RANS model must vanish. The NKE model satisfies this constraint, since  $\tilde{S}_{ii}(t) = 0$  in (30) by virtue of the fact that  $S_{ii}(\tau) = 0$  due to continuity. Secondly, the NKE model reduces to the SKE model in the equilibrium limit of slowly-varying mean strain rate. If  $\Omega_S$  is some frequency that characterizes the rate at which the strain rate is changing in a flow, then as  $\Lambda_m \Omega_S \rightarrow 0$  it can be verified that  $\tilde{S}_{ij}(t) \rightarrow S_{ij}(t)$ . Finally, it should be pointed out that through an analysis of the connection between turbulence and non-Newtonian viscoelastic fluids, Crow<sup>5</sup> obtained a Reynolds stress closure somewhat similar to that used in the NKE model. However, that model assumed an *a priori* connection between turbulence and viscoelasticity that is not needed here.

#### IV. Analytical Tests of the NKE Model

There are several test cases for which the NKE model can be applied analytically. These include the impulsively sheared homogeneous turbulence of Bardina *et al.*<sup>18</sup> and the periodically-sheared turbulence of Yu and Girimaji,<sup>17</sup> for which DNS data exist for comparison with the model results. A third analytical test case is turbulence that is strained, relaxed, and then destrained, for which experimental results using particle image velocimetry (PIV) have recently been reported by Chen *et al.*<sup>19</sup> A final test case involves the interaction between a shock wave and initially homogeneous isotropic turbulence.

In the first three cases, the turbulence is homogeneous and the applied strain varies only in time. The  $k$  and  $\epsilon$  transport equations are thus written in homogeneous form as

$$\frac{\partial k}{\partial t} = P_k - \epsilon \quad \text{and} \quad \frac{\partial \epsilon}{\partial t} = C_{\epsilon 1} P_k \frac{\epsilon}{k} - C_{\epsilon 2} \frac{\epsilon^2}{k}, \quad (32)$$

where  $P_k$  is defined in (18) and the nonequilibrium anisotropy is

$$b_{ij} = -C_\mu \frac{k}{\epsilon} \tilde{S}_{ij}. \quad (33)$$

Calculation of the effective strain rate in (30), where now the integral is with respect to simply  $d\tau$ , closes the coupled system of equations, which can then be integrated numerically. For all test cases, the memory time scale is taken as

$$\Lambda_m = 0.26 \frac{k}{\epsilon}; \quad (34)$$

it will be seen that the prefactor 0.26 gives good agreement with experimental and computational validation results in all test cases.

##### IV.A. Impulsively-Sheared Homogeneous Turbulence

The applied mean strain rate tensor for the homogeneous shear turbulence of Bardina *et al.*<sup>18</sup> is

$$S_{12}(t) = S_{21}(t) = \begin{cases} 0 & \text{for } t < 0 \\ S/2 & \text{for } t > 0 \end{cases}, \quad (35)$$

where all other components of the strain tensor are zero. The resulting effective strain rate for  $t > 0$  is

$$\tilde{S}_{12}(t) = \tilde{S}_{21}(t) = \frac{S}{2} \left[ 1 - e^{-t/\Lambda_m} \right], \quad (36)$$

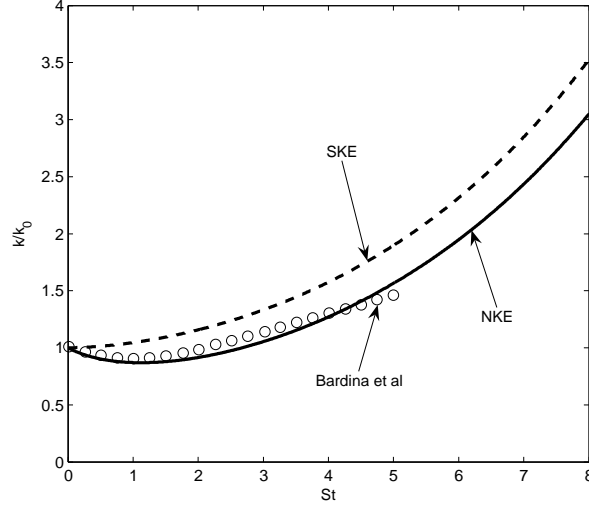


**Figure 5.** Evolution of the turbulent kinetic energy  $k/k_0$  for initially isotropic turbulence that is homogeneously sheared. The new NKE model clearly shows better agreement with the LES data of Bardina *et al.*<sup>18</sup> than the SKE model.

and the anisotropy calculated using (33) is

$$b_{12}(t) = b_{21}(t) = -C_\mu \frac{k}{\epsilon} \frac{S}{2} \left[ 1 - e^{-t/\Lambda_m} \right], \quad (37)$$

where the turbulence for  $t < 0$  is isotropic and  $b_{ij}(t < 0) = 0$ . Note that the SKE model predicts

$$b_{12}(t) = b_{21}(t) = -C_\mu \frac{k}{\epsilon} \frac{S}{2}, \quad (38)$$

and it is thus clear that the anisotropy in the NKE closure is reduced below the SKE result for small times when  $t < \Lambda_m$ .

Integration of Eqs. (32) and (37) from time  $t = 0$  yields the kinetic energy evolution shown in Figure (5) for  $Sk_0/\epsilon_0 = 3.4$ . The inclusion of nonequilibrium effects and the subsequent reduction in the anisotropy magnitude for small times lowers the initial kinetic energy production, resulting in improved agreement with the LES results of Bardina *et al.*<sup>18</sup> For times  $t \gg \Lambda_m$  the nonequilibrium correction to the anisotropy in (37) is negligible and the kinetic energy growth rate is similar to that obtained for the SKE model.

#### IV.B. Periodically-Sheared Turbulence

The applied mean strain rate for the periodically sheared turbulence simulated by Yu and Girimaji<sup>17</sup> is

$$S_{12}(t) = S_{21}(t) = \begin{cases} 0 & \text{for } t < 0 \\ (S_{max}/2) \sin(\omega t) [\delta_{i1}\delta_{j2} + \delta_{i2}\delta_{j1}] & \text{for } t > 0 \end{cases}, \quad (39)$$

where  $\omega$  is the shearing frequency and all other components of the applied mean strain tensor are zero. For  $t > 0$ , the resulting effective strain rate is

$$\tilde{S}_{12}(t) = \tilde{S}_{21}(t) = \frac{1}{(\omega\Lambda_m)^2 + 1} \frac{S_{max}}{2} \left[ \sin(\omega t) - \omega\Lambda_m \left( \cos(\omega t) - e^{-t/\Lambda_m} \right) \right], \quad (40)$$

and the corresponding anisotropy for the nonequilibrium model is

$$b_{12}(t) = b_{21}(t) = -\frac{C_\mu}{(\omega\Lambda_m)^2 + 1} \frac{S_{max}}{2} \frac{k}{\epsilon} \left[ \sin(\omega t) - \omega\Lambda_m \left( \cos(\omega t) - e^{-t/\Lambda_m} \right) \right]. \quad (41)$$

In contrast, the SKE model simply yields an anisotropy of the form

$$b_{12}(t) = b_{21}(t) = -C_\mu \frac{S_{max}}{2} \frac{k}{\epsilon} \sin(\omega t). \quad (42)$$

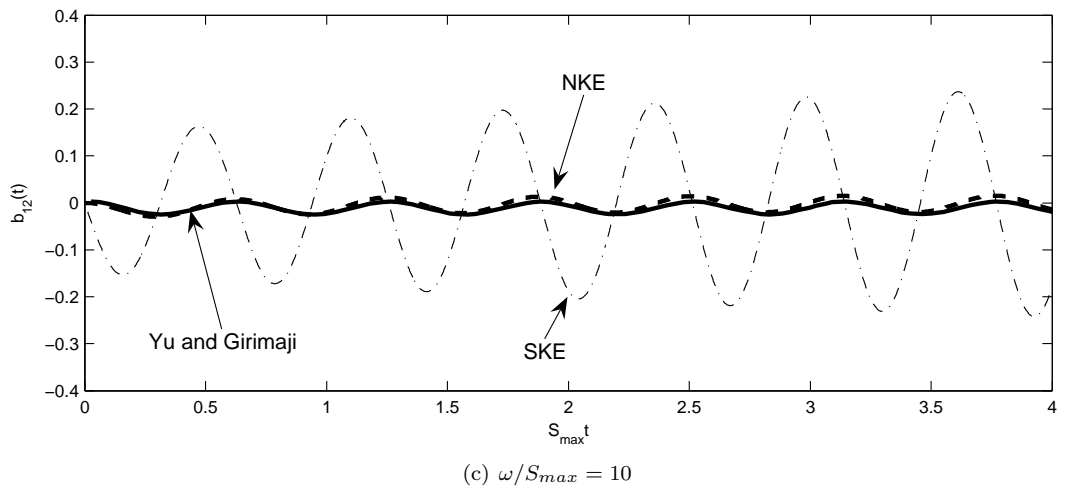
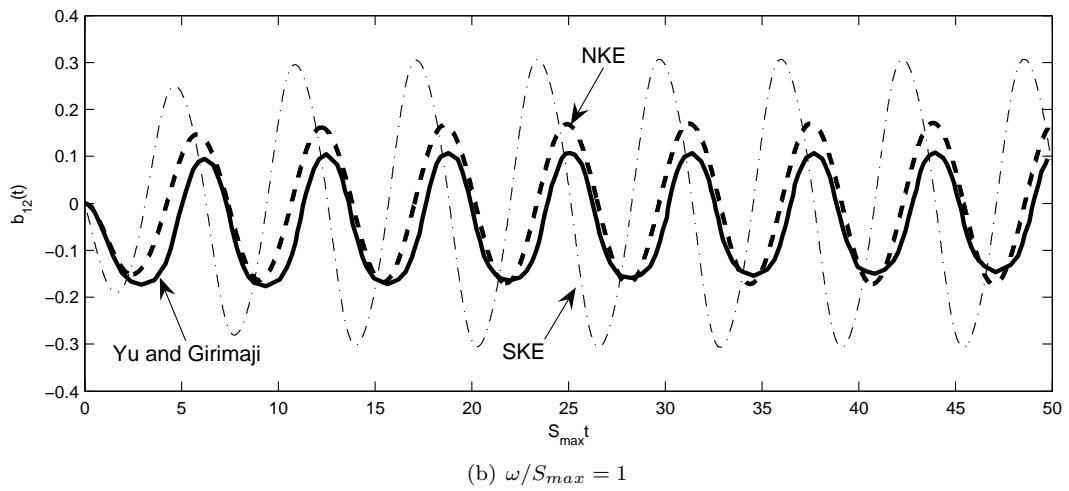
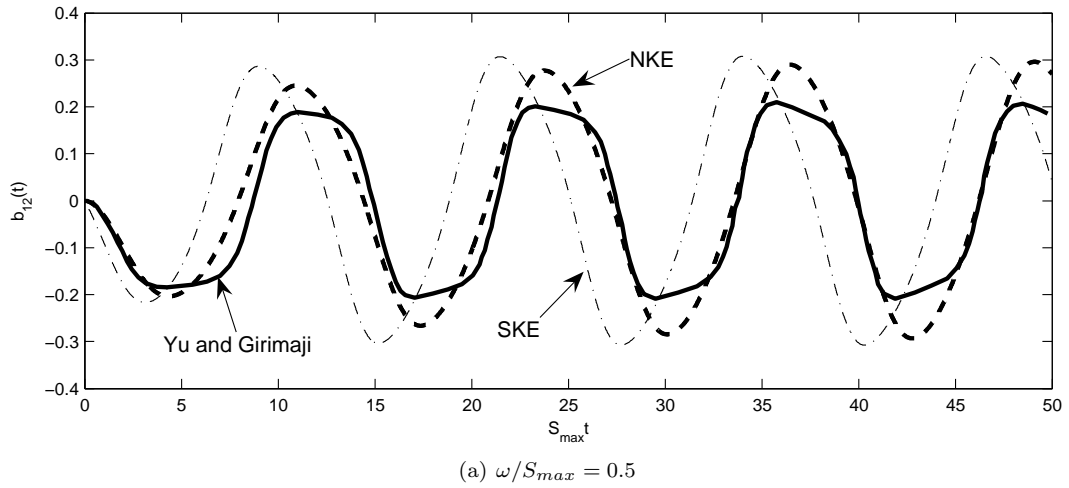
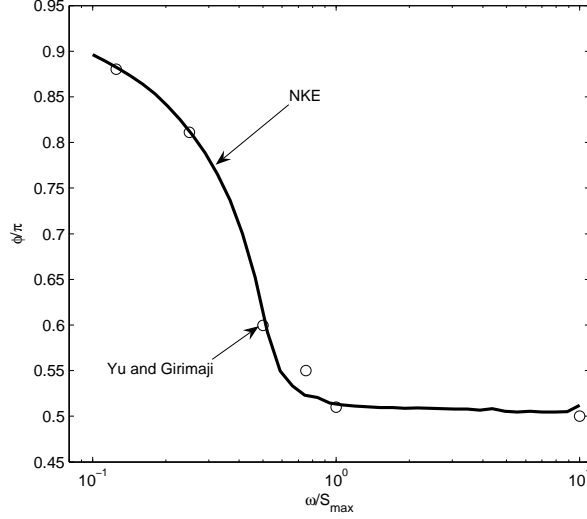


Figure 6. Plot of  $b_{12}$  for periodically sheared turbulence with three different shearing frequencies. In all cases, the NKE model shows better agreement with the computational data of Yu and Girimaji<sup>17</sup> than the SKE model.



**Figure 7.** Phase difference between  $b_{12}$  and the applied shear, where the NKE model agrees well with the Yu and Girimaji<sup>17</sup> results, and the SKE model predicts a constant phase difference of  $\phi/\pi = 1$  independent of the shearing frequency.

The NKE model therefore predicts a decrease in the anisotropy amplitude and an increase in the phase difference with the applied shear as the quantity  $\omega\Lambda_m$  increases. In addition, there is a decaying nonzero offset that also depends on  $\omega\Lambda_m$ . This dependence on the shearing frequency is completely unpredicted by RANS closures that take into account only the instantaneous mean strain tensor, such as the SKE closure in (42).

Periodic shear integration results for shearing frequencies  $\omega/S_{max} = 0.5, 1.0,$  and  $10$  are shown in Figure 6, where  $S_{max}k_0/\epsilon_0 = 3.3$ . Comparison with the DNS results of Yu and Girimaji<sup>17</sup> indicates that the NKE model agrees with the data much more closely than the SKE model. In particular, the anisotropy amplitude for the NKE model is reduced ever more strongly and the phase difference between the applied shear and anisotropy approaches  $\pi/2$  as the shearing frequency increases.

Of considerable interest in periodically-sheared turbulence is the relative phase difference between the anisotropy  $b_{12}$  and the applied shear, since a phase lag between the two results in negative turbulence kinetic energy production. This phase lag reaches a constant value after several shear oscillations, and can be measured accurately for all shearing frequencies by simulating the turbulence to times much greater than  $S_{max}t = 50$ . The resulting phase plot for the NKE model in Figure 7 shows excellent agreement with the Yu and Girimaji results. By comparison, note that the SKE model predicts a constant phase difference of  $\phi/\pi = 1$ , independent of the shearing frequency.

#### IV.C. Straining, Relaxation, and De-Straining of HIT

Turbulence subjected to straining, relaxation, and destraining was recently investigated using PIV by Chen *et al.*<sup>19</sup> The applied strain in those experiments can be represented as

$$S_{11}(t) = -S_{22}(t) = \begin{cases} 0 & \text{for } 0 \leq t \leq t_1 \\ a_1(t - t_1) & \text{for } t_1 < t \leq t_2 \\ -a_2(t - t_3) & \text{for } t_2 < t \leq t_3 \\ 0 & \text{for } t_3 < t \leq t_4 \\ -a_3(t - t_4) & \text{for } t_4 < t \leq t_5 \\ a_4(t - t_6) & \text{for } t_5 < t \leq t_6 \end{cases}, \quad (43)$$

where the  $a_i$  have dimensions of  $1/t^2$  and are chosen, along with the  $t_i$ , to give reasonably good agreement with the experimentally applied strain, as shown in Figure 8. The effective strain rate is again calculated

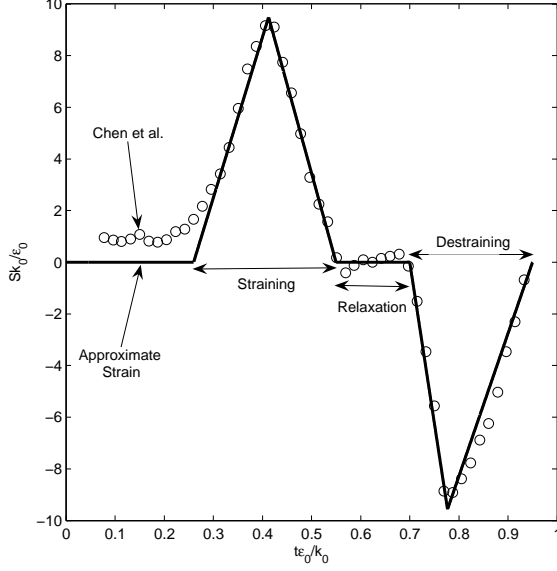


Figure 8. The approximate applied mean strain rate, where good agreement is obtained with the experimental straining-relaxation-destraining cycle of Chen *et al.*<sup>19</sup>

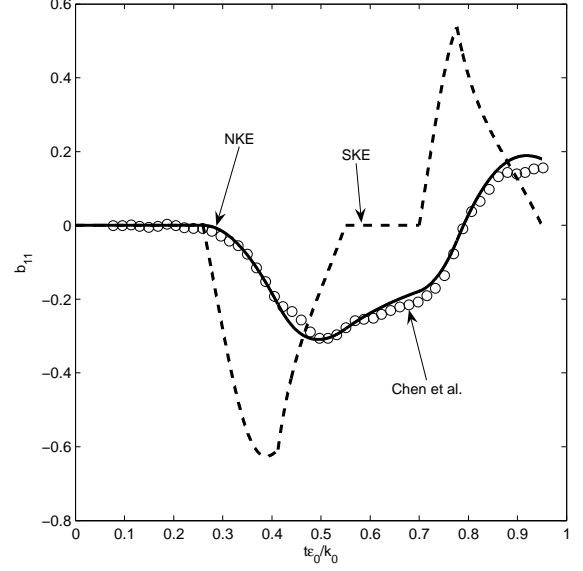


Figure 9. Evolution of  $b_{11}$  as determined by the NKE and SKE models, where it is clear that the NKE model agrees much more closely with the PIV data from Chen *et al.*<sup>19</sup>

using (30) and the resulting piecewise expression is

$$\tilde{S}_{11}(t) = \begin{cases} 0 & \text{for } 0 \leq t \leq t_1 \\ a_1 \Lambda_m (e^{-(t-t_1)/\Lambda_m} - 1) + a_1 (t - t_1) & \text{for } t_1 < t \leq t_2 \\ ((a_1 + a_2)t_2 - a_2 t_3 - a_1 t_1) e^{-(t-t_2)/\Lambda_m} + \Lambda_m (a_1 e^{-(t-t_1)/\Lambda_m} - (a_1 + a_2) e^{-(t-t_2)/\Lambda_m} + a_2) - a_2 (t - t_3) & \text{for } t_2 < t \leq t_3 \\ ((a_1 + a_2)t_2 - a_2 t_3 - a_1 t_1) e^{-(t-t_2)/\Lambda_m} + \Lambda_m (a_1 e^{-(t-t_1)/\Lambda_m} - (a_1 + a_2) e^{-(t-t_2)/\Lambda_m} + a_2 e^{-(t-t_1)/\Lambda_m}) & \text{for } t_3 < t \leq t_4 \\ ((a_1 + a_2)t_2 - a_2 t_3 - a_1 t_1) e^{-(t-t_2)/\Lambda_m} + \Lambda_m (a_1 e^{-(t-t_1)/\Lambda_m} - (a_1 + a_2) e^{-(t-t_2)/\Lambda_m} + a_2 e^{-(t-t_1)/\Lambda_m}) - a_3 \Lambda_m (e^{-(t-t_4)/\Lambda_m} - 1) - a_3 (t - t_4) & \text{for } t_4 < t \leq t_5 \\ ((a_1 + a_2)t_2 - a_2 t_3 - a_1 t_1) e^{-(t-t_2)/\Lambda_m} + \Lambda_m (a_1 e^{-(t-t_1)/\Lambda_m} - (a_1 + a_2) e^{-(t-t_2)/\Lambda_m} + a_2 e^{-(t-t_1)/\Lambda_m}) - ((a_3 + a_4)t_5 - a_4 t_6 - a_3 t_4) e^{-(t-t_5)/\Lambda_m} - \Lambda_m (a_3 e^{-(t-t_4)/\Lambda_m} - (a_3 + a_4) e^{-(t-t_5)/\Lambda_m} + a_4) + a_4 (t - t_6) & \text{for } t_5 < t \leq t_6 \end{cases} . \quad (44)$$

The only nonzero components of the anisotropy are  $b_{11}$  and  $b_{22}$ , for which the NKE closure yields

$$b_{11}(t) = \frac{\overline{u_1' u_1'}}{2k} - \frac{1}{3} = -C_\mu \frac{k}{\epsilon} \tilde{S}_{11}(t) = -b_{22}(t) . \quad (45)$$

Integration of the  $k$  and  $\epsilon$  equations yields the anisotropy evolution shown in Figure 9, where the NKE model shows excellent agreement with the PIV results of Chen *et al.* In particular, the NKE model correctly predicts the slow decay of the anisotropy during the relaxation phase as well as the gradual increase to positive anisotropy during the destraining phase. By comparison, the result from the SKE model in Figure 9 shows far poorer agreement with the experimental data.

#### IV.D. Shock-Turbulence Interaction

The interaction between a shock wave and homogeneous isotropic turbulence is typically modeled as steady and one-dimensional, resulting in the compressible  $k$  and  $\epsilon$  transport equations<sup>20</sup>

$$\rho \bar{u} \frac{\partial k}{\partial x} = -\rho \overline{u' u'} \frac{\partial \bar{u}}{\partial x} - \rho (\epsilon + \epsilon_c) + \overline{p' \theta'} \quad \text{and} \quad \rho \bar{u} \frac{\partial \epsilon}{\partial x} = -C_{\epsilon 1} \rho \overline{u' u'} \frac{\partial \bar{u}}{\partial x} \frac{\epsilon}{k} - C_{\epsilon 2} \frac{\epsilon^2}{k} , \quad (46)$$

where  $\rho$  is the density,  $\epsilon_c$  is the compressible dissipation rate, and  $\overline{p'\theta'}$  is the pressure dilatation term. Following Sinha *et al.*,<sup>20</sup> the dissipation terms  $\epsilon$  and  $\epsilon_c$ , as well as the pressure dilatation, are taken to have a negligible effect on the evolution of  $k$  and  $\epsilon$  across the shock. The resulting transport equations are therefore dominated by kinetic energy production and are written as

$$\overline{u} \frac{\partial k}{\partial x} = -\overline{u'u'} \frac{\partial \overline{u}}{\partial x} \quad \text{and} \quad \overline{u} \frac{\partial \epsilon}{\partial x} = -C_{\epsilon 1} \overline{u'u'} \frac{\partial \overline{u}}{\partial x} \frac{\epsilon}{k}, \quad (47)$$

which can be integrated with respect to  $x$ .

The straining imposed by the shock is represented by a top-hat function of the form

$$S_{11}(x) = \frac{\partial \overline{u}}{\partial x} = \begin{cases} 0 & \text{for } x \leq x_i \\ S & \text{for } x_i < x \leq x_f \\ 0 & \text{for } x_f < x \end{cases}, \quad (48)$$

where  $S$  is the shock strength and  $\delta = x_f - x_i$  is the shock width. In order to properly simulate a shock wave, the shock-turbulence interaction will ultimately be examined in the limit as the shock width  $\delta$  goes to zero.

The effective strain rate integral is written in spatial form as

$$\tilde{S}_{ij}(x) = \int_{-\infty}^x \frac{e^{-(x-\tau)/\Lambda_m}}{\Lambda_m} S_{ij}(\tau) d\tau, \quad (49)$$

where note that  $\Lambda_m$  now has units of length instead of time. For the applied strain in (48), the effective strain rate is

$$\tilde{S}_{11}(x) = \begin{cases} 0 & \text{for } x \leq x_i \\ S [1 - e^{-(x-x_i)/\Lambda_m}] & \text{for } x_i < x \leq x_f \\ S [e^{-(x-x_f)/\Lambda_m} - e^{-(x-x_i)/\Lambda_m}] & \text{for } x_f < x \end{cases}, \quad (50)$$

and the maximum value attained by  $\tilde{S}_{11}$  in the shock region is

$$\tilde{S}_{11}(x_f) = \tilde{S}_{11,max} = S [1 - e^{-\delta/\Lambda_m}]. \quad (51)$$

It is clear from (51) that as the width of the shock becomes small with respect to  $\Lambda_m$ , the maximum value of the effective strain rate in the shock goes to zero. Thus, in the limit as  $\delta/\Lambda_m \rightarrow 0$ , the Reynolds stress predicted by the NKE model becomes simply

$$\overline{u'u'} = \frac{2}{3} k. \quad (52)$$

This is essentially a zero eddy viscosity model of the shock-turbulence interaction, and the  $k$  and  $\epsilon$  transport equations in (47) are easily integrated to obtain

$$\frac{k_2}{k_1} = \left( \frac{\overline{u}_1}{\overline{u}_2} \right)^{2/3} \quad \text{and} \quad \frac{\epsilon_2}{\epsilon_1} = \left( \frac{\overline{u}_1}{\overline{u}_2} \right)^{(2/3)C_{\epsilon 1}}, \quad (53)$$

where subscripts 1 and 2 are the states upstream and downstream of the shock, respectively.

The zero eddy viscosity model gives closer agreement with DNS data<sup>21,22</sup> than either the SKE or RKE models, as shown in Figures 10 and 11. Note however, that further reductions in the eddy viscosity are required to obtain better agreement with the DNS data, and this is not possible in the NKE model. Sinha *et al.* were able to obtain improved agreement by considering shock unsteadiness,<sup>20</sup> and it is possible that the NKE model could be extended in the future to account for this effect.

## V. Full Realizability

The NKE model

$$b_{ij} = -C_{\mu} \frac{\tilde{S} k}{\epsilon} \frac{\tilde{S}_{ij}}{\tilde{S}} \quad (54)$$

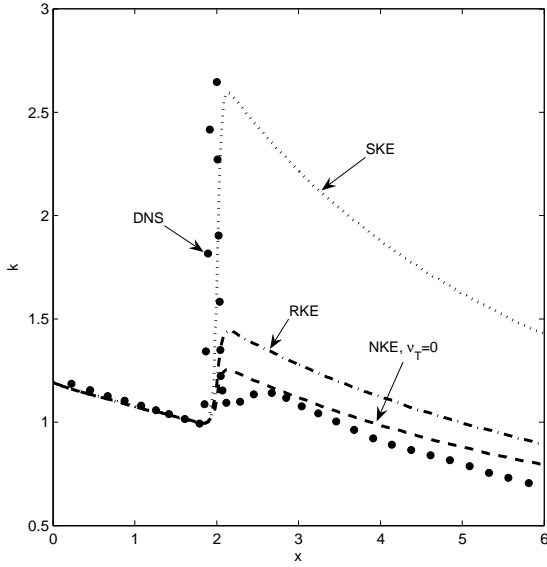


Figure 10. Spatial turbulent kinetic energy evolution for  $M_1 = 1.29$  in the shock-turbulence interaction (plot reproduced from Sinha *et al.*<sup>20</sup>).

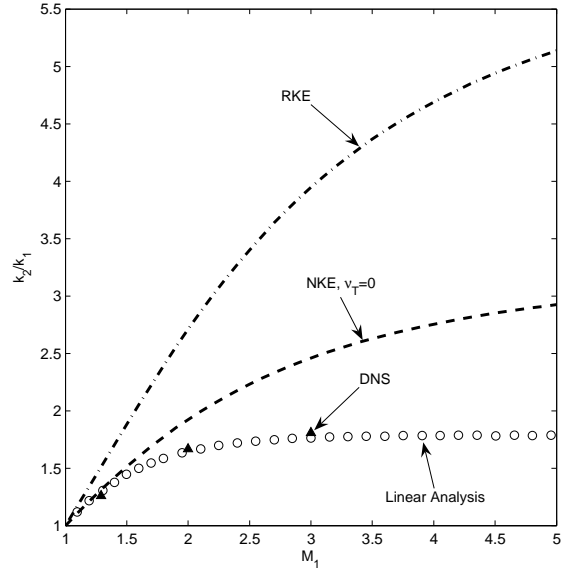


Figure 11. Kinetic energy amplification across a shock as a function of upstream Mach number.

can also be made fully realizable. Note that in this regard, the distinction between the SKE model in (12) and the NKE model is irrelevant. Following the basic approach used in the realizable  $k - \epsilon$  (RKE) model but changing the formulation slightly, the anisotropy is allowed to depend on a general function of  $\tilde{S}k/\epsilon$  such that

$$b_{ij} = -f\left(\frac{\tilde{S}k}{\epsilon}\right) \frac{\tilde{S}_{ij}}{\tilde{S}}. \quad (55)$$

For small  $\tilde{S}k/\epsilon$  the agreement with the channel flow computational data in Figure 1 indicates that the closure in (54) holds and

$$f\left(\frac{\tilde{S}k}{\epsilon}\right) = C_\mu \frac{\tilde{S}k}{\epsilon} \quad \text{as} \quad \frac{\tilde{S}k}{\epsilon} \rightarrow 0. \quad (56)$$

For large  $\tilde{S}k/\epsilon$ , Figure 2 and the RKE model motivate an anisotropy independent of  $\tilde{S}k/\epsilon$  such that

$$f\left(\frac{\tilde{S}k}{\epsilon}\right) = C_\infty \quad \text{as} \quad \frac{\tilde{S}k}{\epsilon} \rightarrow \infty, \quad (57)$$

where  $C_\infty$  is a constant. This large  $\tilde{S}k/\epsilon$  limit is also consistent with the quasi-Lagrangian picture of turbulence anisotropy, since for large  $\tilde{S}k/\epsilon$  the vortical structures become completely aligned and the anisotropy magnitude approaches a constant finite value associated with the maximum alignment.

Thus the anisotropy function  $f(\tilde{S}k/\epsilon)$  is written in piecewise form as

$$f\left(\frac{\tilde{S}k}{\epsilon}\right) = \begin{cases} C_\mu \frac{\tilde{S}k}{\epsilon} & \text{as} \quad \frac{\tilde{S}k}{\epsilon} \rightarrow 0 \\ C_\infty & \text{as} \quad \frac{\tilde{S}k}{\epsilon} \rightarrow \infty \end{cases}. \quad (58)$$

However, this function only renders the anisotropy model in (55) realizable, not fully realizable. To be fully realizable, the anisotropy model must be able to access all regions of the Lumley turbulent state triangle<sup>23</sup> in Figure 12, where the three invariants of the anisotropy tensor are

$$I_b = b_{ii}, \quad -II_b = \frac{1}{2}b_{ij}b_{ji} \quad \text{and} \quad III_b = \frac{1}{3}b_{ij}b_{jk}b_{ki}, \quad (59)$$

and the allowable turbulence states are bounded by

- i.  $-II_b \leq \frac{1}{9} + 3III_b$ ,
- ii.  $-II_b \geq \pm 3\left(\frac{1}{2}III_b\right)^{2/3}$ .

Any turbulence model that produces deviatoric stresses corresponding to anisotropy states  $(III_b, -II_b)$  outside these bounds is predicting physically unrealizable state of turbulence. At the same time, any turbulence model that cannot produce all possible states  $(III_b, -II_b)$  within the turbulent state triangle (such as the RKE model) is unable to represent all physically realizable turbulence states. Through the correct definition of the constant  $C_\infty$  in the equilibrium anisotropy function  $f(\tilde{S}k/\epsilon)$ , it is possible to obtain a fully-realizable model that remains bounded within the turbulent state triangle and is at the same time able to access all possible states within the triangle.

Using the general anisotropy model in (55), the second and third anisotropy tensor invariants are

$$-II_b = \frac{1}{2}b_{ij}b_{ji} = \frac{1}{2}f^2 \quad \text{and} \quad III_b = \frac{1}{3}b_{ij}b_{jk}b_{ki} = -\frac{1}{3}\beta f^3. \quad (60)$$

The variable  $\beta$  is related to the second and third invariants of the mean strain rate tensor and is written

$$\beta = \frac{\tilde{S}_{ij}\tilde{S}_{jk}\tilde{S}_{ki}}{\tilde{S}^3}. \quad (61)$$

Since  $-II_b$  and  $III_b$  are completely determined by  $\beta$  and  $f$ , it is possible to conduct the realizability analysis purely in terms of these variables. Thus, rather than restricting  $II_b$  and  $III_b$  as in i. and ii., equivalent restrictions are placed on the allowable values of  $\beta$  and  $f$ .

Realizability bounds on the value of  $\beta$  are determined from realizability condition ii, which yields

$$-\frac{1}{\sqrt{6}} \leq \beta \leq \frac{1}{\sqrt{6}}. \quad (62)$$

These bounds effectively ensure that the turbulence states predicted by (55) always remain within the left and right sides of the turbulent state triangle in Figure 12, though they do not ensure that the states remain below the upper limit of the triangle. For this, realizability must be imposed on the maximum allowable value of  $f$ , which is equivalent to limiting the maximum degree of anisotropy. Since maximum anisotropy occurs in the high  $\tilde{S}k/\epsilon$  limit where  $f(\tilde{S}k/\epsilon) = C_\infty$ , it is through the upper bound on  $f$  that an appropriate value for  $C_\infty$  is defined.

From realizability constraint i., we obtain a conditional equation for  $f$  of the form

$$\beta f^3 + \frac{1}{2}f^2 - \frac{1}{9} \leq 0. \quad (63)$$

For a given value of  $\beta$ , this cubic relation is solved by defining the parameter

$$\theta = \cos^{-1} \left[ \left( \frac{12}{\beta} - \frac{1}{\beta^3} \right) |\beta|^3 \right], \quad (64)$$

where for  $\beta > 0$

$$f \leq \frac{1}{3\beta} \cos\left(\frac{\theta}{3}\right) - \frac{1}{6\beta}, \quad (65)$$

and for  $\beta < 0$

$$f \leq -\frac{1}{3\beta} \cos\left(\frac{\theta + 4\pi}{3}\right) - \frac{1}{6\beta}. \quad (66)$$

Note that in order for  $\theta$  to be defined,  $\beta$  must be bounded as in (62). If  $\beta = 0$  then equation (63) is no longer cubic and the upper bound on  $f$  is

$$f \leq \sqrt{\frac{2}{9}}. \quad (67)$$

For a given value of  $\beta$ , these expressions provide upper bounds on the anisotropy magnitude  $f$  allowed by realizability. In the sense that  $C_\infty$  is the degree of anisotropy in the high  $\tilde{S}k/\epsilon$ , maximum anisotropy limit,

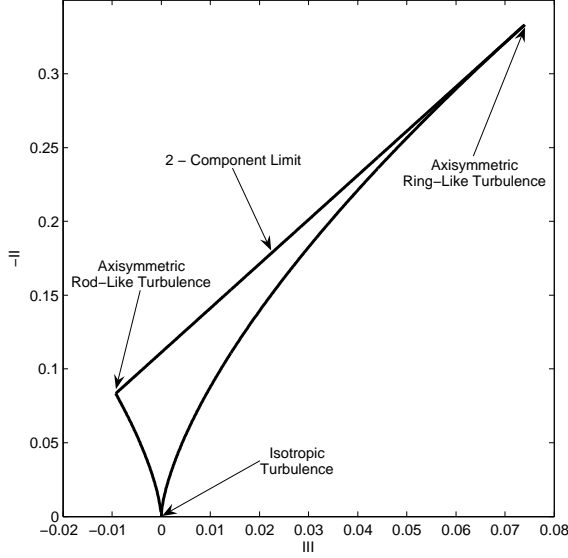


Figure 12. The turbulent state triangle<sup>23</sup> in anisotropy tensor invariant coordinates  $-II_b$  and  $III_b$ .

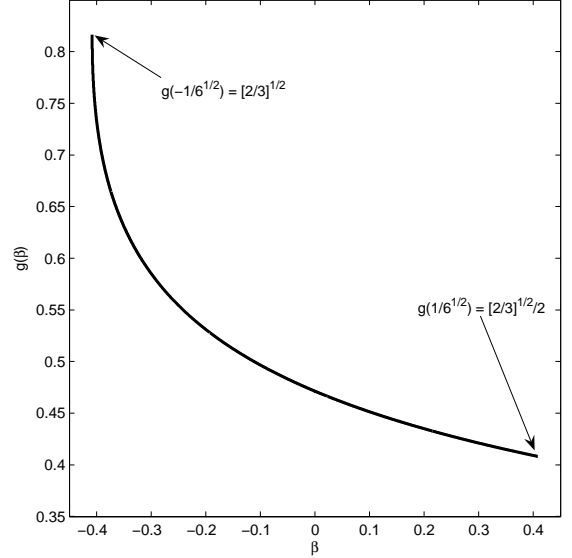


Figure 13. The function  $g(\beta)$  plotted versus  $\beta$  with upper and lower limits on  $\beta$  and  $g(\beta)$  indicated.

we define  $C_\infty \equiv g(\beta)$ , where

$$g(\beta) = \begin{cases} -\frac{1}{3\beta} \cos\left(\frac{\theta+4\pi}{3}\right) - \frac{1}{6\beta} & \text{for } \beta < 0 \\ \sqrt{\frac{2}{9}} & \text{for } \beta = 0 \\ \frac{1}{3\beta} \cos\left(\frac{\theta}{3}\right) - \frac{1}{6\beta} & \text{for } \beta > 0 \end{cases} . \quad (68)$$

This function is plotted versus  $\beta$  in Figure 13, where it is clear that the upper and lower bounds on  $g(\beta)$  correspond to the two limits on  $\beta$  in (62).

Thus, the requirement of full realizability sets the constant  $C_\infty$  appearing in (55), and the anisotropy magnitude is now written as

$$f\left(\frac{\tilde{S}k}{\epsilon}, \beta\right) = \begin{cases} C_\mu \frac{\tilde{S}k}{\epsilon} & \text{for } 0 \leq \frac{\tilde{S}k}{\epsilon} \leq \frac{g(\beta)}{C_\mu} \\ g(\beta) & \text{for } \frac{g(\beta)}{C_\mu} < \frac{\tilde{S}k}{\epsilon} < \infty \end{cases} , \quad (69)$$

where  $g(\beta)$  is defined in (68) and  $\theta$  is defined in (64).

## VI. Additional Considerations

The explicit history integral that accounts for nonequilibrium effects in the NKE model is acceptable for model validation on test cases that permit an analytical solution, such as in Section IV, but implementing the model in a CFD code requires that only local, instantaneous variables can be used. To accommodate this, the term  $S_{ij}(\tau)$  appearing in the effective strain integral can be Taylor expanded in a Lagrangian sense about the current time  $t$  as

$$S_{ij}(\tau) = S_{ij}(t) - S_{ij}^\nabla \Big|_t (t - \tau) + \frac{1}{2} S_{ij}^{\nabla^2} \Big|_t (t - \tau)^2 + \dots , \quad (70)$$

where  $S_{ij}^\nabla$  denotes the Jaumann derivative, defined as

$$S_{ij}^\nabla = \frac{DS_{ij}}{Dt} + S_{ik}\Omega_{kj} - \Omega_{ik}S_{kj} , \quad (71)$$

and

$$\Omega_{ij} = \frac{1}{2} \left( \frac{\partial \bar{u}_i}{\partial x_j} - \frac{\partial \bar{u}_j}{\partial x_i} \right) \quad (72)$$

is the mean rotation rate tensor. Whereas the material derivative  $DS_{ij}/Dt$  describes the change of the strain rate tensor in a fluid element translating with the mean flow, the Jaumann derivative additionally accounts for changes in the strain tensor due to rotation of the fluid element by the flow.

Employing the Lagrangian Taylor expansion in (70), the effective strain rate integral in (30) is written

$$\tilde{S}_{ij}(t) = \int_{-\infty}^t \frac{e^{-(t-\tau)/\Lambda_m}}{\Lambda_m} \left[ S_{ij}(t) - S_{ij}^{\nabla} \Big|_t (t-\tau) + \frac{1}{2} S_{ij}^{\nabla^2} \Big|_t (t-\tau)^2 + \dots \right] D\tau. \quad (73)$$

Since all of the derivatives of  $S_{ij}$  depend on  $t$  only, it is possible to write

$$\tilde{S}_{ij}(t) = S_{ij}(t) + \sum_{n=1}^{\infty} \frac{(-1)^n}{n!} S_{ij}^{\nabla^n} \Big|_t \int_{-\infty}^t (t-\tau)^n \frac{e^{-(t-\tau)/\Lambda_m}}{\Lambda_m} d\tau, \quad (74)$$

and evaluating the moments of the history function in the integral, we finally obtain the expression

$$\tilde{S}_{ij}(t) = S_{ij}(t) + \sum_{n=1}^{\infty} (-\Lambda_m)^n S_{ij}^{\nabla^n} \Big|_t. \quad (75)$$

It is computationally impractical to calculate all higher order Jaumann derivatives of the strain rate tensor, so only the  $n = 1$  term is retained, yielding an approximate expression for the effective strain rate

$$\tilde{S}_{ij}(t) \approx S_{ij}(t) - C_{\Lambda} \frac{k}{\epsilon} S_{ij}^{\nabla} \Big|_t = S_{ij} - C_{\Lambda} \frac{k}{\epsilon} \left( \frac{DS_{ij}}{Dt} + S_{ik}\Omega_{kj} - \Omega_{ik}S_{kj} \right). \quad (76)$$

This representation of the effective strain rate replaces the integral form in (30), thereby rendering the NKE model described by Eqs. (29)-(31) suitable for implementation in RANS modeling codes.

The fully-realizable nonequilibrium NKE turbulence closure model is thus summarized by the following set of equations:

$$\begin{aligned} \overline{u'_i u'_j} &= \frac{2}{3} k \delta_{ij} - 2kf \left( \frac{\tilde{S}k}{\epsilon}, \beta \right) \frac{\tilde{S}_{ij}}{\tilde{S}} \\ \tilde{S}_{ij}(t) &\approx S_{ij}(t) - C_{\Lambda} \frac{k}{\epsilon} \left( \frac{DS_{ij}}{Dt} + S_{ik}\Omega_{kj} - \Omega_{ik}S_{kj} \right) \\ \tilde{S} &= \sqrt{\tilde{S}_{ij}\tilde{S}_{ji}}; \quad \beta = \frac{\tilde{S}_{ij}\tilde{S}_{jk}\tilde{S}_{ki}}{\tilde{S}^3} \\ f \left( \frac{\tilde{S}k}{\epsilon}, \beta \right) &= \begin{cases} C_{\mu} \frac{\tilde{S}k}{\epsilon} & \text{for } 0 \leq \frac{\tilde{S}k}{\epsilon} \leq \frac{g(\beta)}{C_{\mu}} \\ g(\beta) & \text{for } \frac{g(\beta)}{C_{\mu}} < \frac{\tilde{S}k}{\epsilon} < \infty \end{cases} \\ g(\beta) &= \begin{cases} -\frac{1}{3\beta} \cos\left(\frac{\theta+4\pi}{3}\right) - \frac{1}{6\beta} & \text{for } \beta < 0 \\ \sqrt{\frac{2}{9}} & \text{for } \beta = 0 \\ \frac{1}{3\beta} \cos\left(\frac{\theta}{3}\right) - \frac{1}{6\beta} & \text{for } \beta > 0 \end{cases} \\ \theta &= \cos^{-1} \left[ \left( \frac{12}{\beta} - \frac{1}{\beta^3} \right) |\beta|^3 \right] \end{aligned} \quad (77)$$

where the  $k$  and  $\epsilon$  transport equations from the SKE model close the system of equations, with  $C_{\Lambda} = 0.26$  and  $C_{\mu} = 0.09$ . Despite the fact that the NKE model above involves several additional equations when compared to traditional two-equation closures such as the SKE model, it can be relatively easily implemented in CFD codes. Once the effective strain rate tensor is calculated, all other relations in (77) are algebraic and straightforward.

Lastly, we note that the NKE model in (77) indirectly bears some similarities to certain types of NLEVMs (*e.g.*, Speziale,<sup>12</sup> Yakhot *et al.*,<sup>13</sup> Yoshizawa and Nisizima,<sup>14</sup> and Huang and Rajagopal<sup>15</sup>). The link between these NLEVMs, which are derived on entirely different grounds, and the NKE model enters through the

Taylor expanded approximate effective strain rate. The NKE model can also be connected to more traditional NLEVMs, where the low  $\tilde{S}k/\epsilon$  form of the Reynolds stress closure in (77) is written explicitly as

$$\overline{u'_i u'_j} = \frac{2}{3}k\delta_{ij} - 2C_\mu \frac{k^2}{\epsilon} \tilde{S}_{ij} = \frac{2}{3}k\delta_{ij} - 2C_\mu \frac{k^2}{\epsilon} S_{ij} + 2C_\mu C_\Lambda \frac{k^3}{\epsilon^2} \left( \frac{DS_{ij}}{Dt} + S_{ik}\Omega_{kj} - \Omega_{ik}S_{kj} \right). \quad (78)$$

The material derivative of  $S_{ij}$  can be expanded using the transport equation for  $S_{ij}$ , which is derived from the RANS equations as

$$\frac{DS_{ij}}{Dt} = -S_{ik}S_{kj} - \Omega_{ik}\Omega_{kj} - \Pi_{ij} + \nu\nabla^2 S_{ij} - \frac{1}{2} \frac{\partial}{\partial x_k} \left( \frac{\partial \overline{u'_i u'_k}}{\partial x_j} + \frac{\partial \overline{u'_j u'_k}}{\partial x_i} \right), \quad (79)$$

where  $\Pi_{ij}$  is the pressure hessian

$$\Pi_{ij} = \frac{1}{\rho} \frac{\partial \bar{p}}{\partial x_i \partial x_j}. \quad (80)$$

For simplicity the last three terms in (79) are defined as

$$F_{ij} \equiv -\Pi_{ij} + \nu\nabla^2 S_{ij} - \frac{1}{2} \frac{\partial}{\partial x_k} \left( \frac{\partial \overline{u'_i u'_k}}{\partial x_j} + \frac{\partial \overline{u'_j u'_k}}{\partial x_i} \right) \quad (81)$$

so that equation (79) is written

$$\frac{DS_{ij}}{Dt} = -S_{ik}S_{kj} - \Omega_{ik}\Omega_{kj} + F_{ij}. \quad (82)$$

The resulting Reynolds stress closure in the low  $\tilde{S}k/\epsilon$  limit is then

$$\overline{u'_i u'_j} = \frac{2}{3}k\delta_{ij} - 2C_\mu \frac{k^2}{\epsilon} S_{ij} - 2C_\mu C_\Lambda \frac{k^3}{\epsilon^2} (S_{ik}S_{kj} + \Omega_{ik}\Omega_{kj} - S_{ik}\Omega_{kj} + \Omega_{ik}S_{kj} - F_{ij}). \quad (83)$$

The expansion can be continued to even higher order by including additional terms in the expression for the effective strain rate. It is the appearance of the second-order products of the strain rate and rotation rate tensors above that is of interest in this connection, since terms of this type are commonly found in nonlinear eddy viscosity models (NLEVMs). Thus the present consideration of nonequilibrium turbulence effects has led to a model that reveals implicit connections to some existing nonlinear Reynolds stress closures, but in general should be able to address much deeper nonequilibrium effects than do these previous models.

## VII. Conclusion

Through an analysis of the physics underlying turbulence anisotropy in the equilibrium and nonequilibrium limits, a new physically-based, fully-realizable, nonequilibrium  $k - \epsilon$  RANS model has been developed. In four distinctly different test cases for which the nonequilibrium history integral can be evaluated analytically, this new closure model shows dramatically improved agreement with experimental and computational data when compared with the SKE model. For the test cases considered, good agreement was obtained without the need to vary any model parameters. In particular, the formulation of the memory time scale  $\Lambda_m$  was identical for all flows examined, introducing the possibility that the new model may be closer to achieving universal accuracy than current models. Moreover, the introduction of a nonequilibrium effective strain rate allows this new model to be applied within a similar framework as currently used for two-equation eddy viscosity models, thereby permitting relatively simple implementation in existing CFD codes.

## Acknowledgement

This work was jointly supported, in part, by the National Aeronautics & Space Administration (NASA) Marshall and Glenn Research Centers and the Department of Defense (DoD) within the NASA Constellation University Institutes Project (CUIP) Space Vehicle Technology Institute (SVTI) under Grant No. NCC3-989, with Claudia Meyer as the project manager.

## References

- <sup>1</sup>Launder, B. E. and Spalding, D. B., "The numerical computation of turbulent flows." *Comp. Meth. App. Mech. Eng.*, Vol. 3, 1974, pp. 269–289.
- <sup>2</sup>Speziale, C. G., "Analytical methods for the development of Reynolds-stress closures in turbulence." *Annu. Rev. Fluid Mech.*, Vol. 23, 1991, pp. 107–157.
- <sup>3</sup>Gatski, T. B. and Jongen, T., "Nonlinear eddy viscosity and algebraic stress models for solving complex turbulent flows." *Prog. Aero. Sci.*, Vol. 36, 2000, pp. 655–682.
- <sup>4</sup>Davidson, P. A., *Turbulence: An Introduction for Scientists and Engineers*, Oxford University Press, 2004.
- <sup>5</sup>Crow, S. C., "Viscoelastic properties of fine-grained incompressible turbulence." *J. Fluid Mech.*, Vol. 33, 1968, pp. 1–20.
- <sup>6</sup>Lumley, J. L., "Toward a turbulent constitutive relation." *J. Fluid Mech.*, Vol. 41, 1970, pp. 413–434.
- <sup>7</sup>Gatski, T. B., "Constitutive equations for turbulent flows." *Theoret. Comput. Fluid Dynamics*, Vol. 18, 2004, pp. 345–369.
- <sup>8</sup>Shih, T. H., Zhu, J., and Lumley, J. L., "A new Reynolds stress algebraic equation model." *Comput. Methods. Appl. Mech. Engrg.*, Vol. 125, 1995, pp. 287–302.
- <sup>9</sup>Gatski, T. B. and Speziale, C. G., "On algebraic stress models for complex turbulent flows." *J. Fluid Mech.*, Vol. 254, 1993, pp. 59–78.
- <sup>10</sup>Johansson, A. V., "Engineering turbulence models and their development, with emphasis on explicit algebraic Reynolds stress models." *Theories of Turbulence - CISM Courses and Lectures - No. 442*, Vol. Springer, 2002, pp. 253–300.
- <sup>11</sup>Craft, T. J., Launder, B. E., and Suga, K., "Development and application of a cubic eddy-viscosity model of turbulence." *Int. J. Heat and Fluid Flow*, Vol. 17, 1996, pp. 108–115.
- <sup>12</sup>Speziale, C. G., "On nonlinear  $K-l$  and  $K-\epsilon$  models of turbulence." *J. Fluid Mech.*, Vol. 178, 1987, pp. 459–475.
- <sup>13</sup>Yakhot, V., Orszag, S. A., Thangam, S., Gatski, T. B., and Speziale, C. G., "Development of turbulence models for shear flows by a double expansion technique." *Phys. Fluids A*, Vol. 4 (7), 1992, pp. 1510–1520.
- <sup>14</sup>Yoshizawa, A. and Nisizima, S., "A nonequilibrium representation of the turbulent viscosity based on a two-scale turbulence theory." *Phys. Fluids A*, Vol. 5 (12), 1993, pp. 3302–3304.
- <sup>15</sup>Huang, Y. N. and Rajagopal, K. R., "On a generalized nonlinear  $K-\epsilon$  model for turbulence that models relaxation effects." *Theoret. Comput. Fluid Dynamics*, Vol. 8, 1996, pp. 275–288.
- <sup>16</sup>Kim, J., Moin, P., and Moser, R., "Turbulence statistics in fully developed channel flow at low Reynolds number." *J. Fluid Mech.*, Vol. 177, 1987, pp. 133–166.
- <sup>17</sup>Yu, D. and Girimaji, S. S., "Direct numerical simulations of homogeneous turbulence subject to periodic shear." *J. Fluid Mech.*, Vol. 566, 2006, pp. 117–151.
- <sup>18</sup>Bardina, J., Ferziger, J. H., and Reynolds, W. C., "Improved turbulence models based on large-eddy simulation of homogeneous, incompressible turbulent flows." *Rep. No. TF-19*, 1983, pp. Stanford Univ.
- <sup>19</sup>Chen, J., Meneveau, C., and Katz, J., "Scale interactions of turbulence subjected to a straining-relaxation-destraining cycle." *J. Fluid Mech.*, Vol. 562, 2006, pp. 123–150.
- <sup>20</sup>Sinha, K., Mahesh, K., and Candler, G. V., "Modeling shock unsteadiness in shock/turbulence interaction." *Phys. Fluids*, Vol. 15 (8), 2003, pp. 2290–2297.
- <sup>21</sup>Mahesh, K., Lele, S. K., and Moin, P., "The influence of entropy fluctuations on the interaction of turbulence with a shock wave." *J. Fluid Mech.*, Vol. 334, 1997, pp. 353.
- <sup>22</sup>Lee, S., Lele, S. K., and Moin, P., "Interaction of isotropic turbulence with shock waves: Effect of shock strength." *J. Fluid Mech.*, Vol. 340, 1997, pp. 225.
- <sup>23</sup>Lumley, J. L., "Computational modeling of turbulent flows." *Adv. Appl. Mech.*, Vol. 18, 1978, pp. 123.